HYDROLIGHT TECHNICAL NOTE 10

INTERPRETATION OF RAMAN SCATTERING COMPUTATIONS

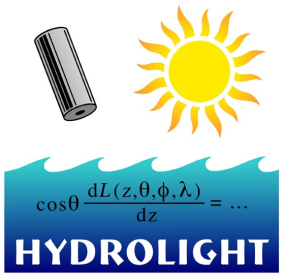

Curtis Mobley **January 2012**

HydroLight Technical Note 9 of December 2010 describes new options for input of user-defined sun and sky irradiances, including an option for simulation of lidar-induced inelastic scatter that I illustrated via a HydroLight simulation of Raman scatter induced by a 488 nm lidar and a hand-check on the H calculation. That simulation led to a question from one reader about the interpretation of solar-induced Raman scatter because my hand-check of the lidar simulation did not seem to agree with H output with solar stimulation. A couple of other users have posed additional questions about Raman scatter. The present note is strives to clarify this confusing business.

One difficulty in interpreting H inelastic scatter output arises because the mathematics of inelastic scatter is formulated in terms of how one particular wavelength scatters to another particular wavelength, whereas H runs use finite wavelength bands and Raman scattered light in one band usually comes from several other bands. H simulations of solar-induced inelastic scatter thus integrate both the excitation and emission wavelengths over finite wavelength bands. I will illustrate this with Raman scatter, but the same complications apply to chlorophyll or CDOM fluorescence. For completeness, I repeat here some of H Tech Note 9 and the Raman section of *Light and Water* (L&W).

Quantities Defining Raman Scatter

The quantities needed to compute Raman scatter contributions to the radiance are

- the Raman scattering coefficient $b^R(\lambda')$, with units of m^{-1}
- the Raman scattering phase function $\tilde{\beta}^R(\psi)$, with units of sr^{-1}
- the Raman wavelength distribution function $f^R(\lambda',\lambda)$, with units of nm^{-1}

We next review each of these quantities in turn.

The Raman scattering coefficient

$b^R(\lambda')$ tells how much of the irradiance at the excitation wavelength λ' scatters into *all* emission wavelengths λ, per unit of distance traveled by the excitation irradiance. The most recently

published values of $b^R(\lambda'=488\text{ nm})$ for water are $(2.7 \pm 0.2)\times10^{-4}$ m^{-1} (Bartlett et al., 1998) and 2.4×10^{-4} m^{-1} (Desiderio, 2000). The current version (5.1.4) of HydroLight uses $b^R(\lambda'=488\text{ nm}) = 2.6\times10^{-4}$ m^{-1} as the default value (this value can be changed on the "Change Defaults" form of the User Interface).

Various values for the wavelength dependence of b^R can be found in the literature. Haltrin and Kattawar (1993, their Eq. A3) use $b^R(\lambda) = b^R(400)(400/\lambda)^4$ when expressed in terms of the *emission* wavelength λ; Ge et al. (1993) use $b^R(\lambda) = b^R(488)(488/\lambda)^5$. Bartlett et al. (1998) reviewed the wavelength dependence of the Raman scattering coefficient in detail and found, based on their measurements, a wavelength dependence of $\lambda^{-4.8\pm0.3}$ for calculations performed in *energy units* (as in HydroLight). In terms of the *excitation* wavelength, Bartlett et al. found $b^R(\lambda') = b^R(488)(488/\lambda')^{5.5\pm0.4}$ for energy computations. The current version 5.1.4 of HydroLight uses $b^R(\lambda') = b^R(488)(488/\lambda')^{5.5}$ as the default (this value can be changed on the "Change Defaults" form of the User Interface). For calculations in terms of *photon numbers* (as in a Monte Carlo simulation), Bartlett et al. found wavelength dependencies of $(\lambda')^{-5.3\pm0.3}$ or $(\lambda)^{-4.6\pm0.3}$.

The Raman phase function

$\tilde{\beta}^R(\psi)$ gives the angular distribution of the scattered radiance. This function is given by L&W (5.91):

$$\tilde{\beta}^R(\psi) = 0.067\,(1 + 0.55\cos^2\psi)\,, \tag{1}$$

where ψ is the scattering angle between the direction of the incident and scattered radiance.

The Raman wavelength distribution function

$f^R(\lambda',\lambda)$ relates the excitation and emission wavelengths, e.g., what wavelengths λ receive the scattered spectral irradiance for a given excitation wavelength λ' or, conversely, what wavelengths λ' excite a given emission wavelength λ. The wavelength distribution function $f^R(\lambda', \lambda)$ is given by Eq. (L&W 5.94, corrected) of Appendix A.

The wavelength distribution function $f^R(\lambda',\lambda)$ was first used with a fixed excitation wavelength of $\lambda' = 488$ nm to generate the corresponding distribution of emission wavelengths, which is plotted in red in Fig. 1. The figure shows that for $\lambda' = 488$ nm, the emission band is centered near 583 nm and has a full width at half max (FWHM) of $\Delta\lambda \approx 15$ nm. The function was then used with a fixed emission wavelength of $\lambda = 583$ nm to generate the corresponding distribution of excitation wavelengths, which is plotted in blue in the figure. The band of wavelengths that contribute to 583 nm is centered near 488 nm and has a FWHM of $\Delta\lambda' \approx 10$ nm.

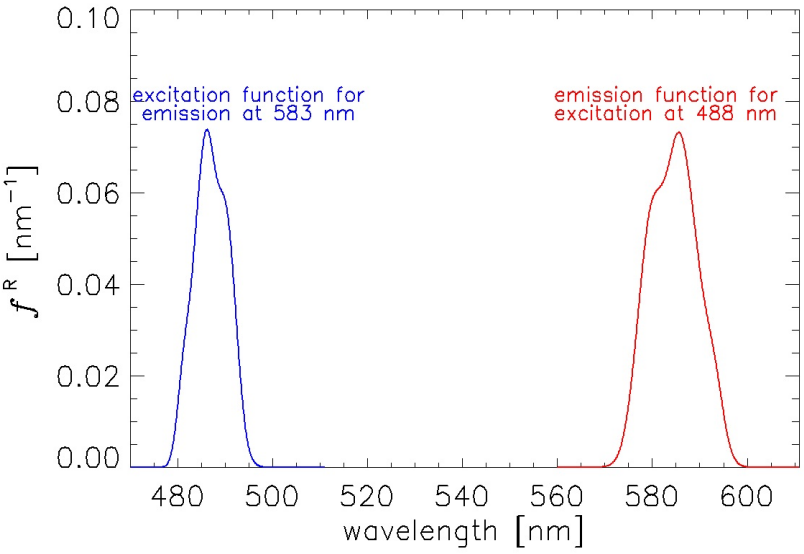

Fig. 1. Raman emission function for excitation at 488 nm (red), and excitation function for emission at 583 nm (blue). Compare with similar figures in Ge et al. (1993; their Fig 3) and Kattawar as Xu (1992; their Fig. 2).

Simulation of Lidar-Induced Raman Scatter

A series of EcoLight (which is much faster than HydroLight and gives the same irradiances and nadir- and zenith-viewing radiances) version 5.1.4 runs was made using the option described in H Tech Note 9 for input of a lidar beam at a single wavelength in an otherwise black sky. The run inputs were

E_d(direct beam) = 1 W m^{-2} at 488 nm; the sky was otherwise black (the input sky irradiance file is HE5/data/examples/Sky_Irrad_Example_Lidar488.txt)
chlorophyll concentration = 0.05 mg m^{-3} in the new Case 1 IOP model
infinitely deep water with the RTE solved down to 50 m
470 to 610 nm with output bands of 1, 5, and 10 nm (3 separate runs)

Figure 2 shows the nadir-viewing water-leaving radiances L_w computed by these EcoLight runs. There are several things to note about these results. First, the fine structure of the Raman output is seen only at 1 nm resolution; 5 or 10 nm resolution blurs out the detailed shape of the emission function. However, the integrated values of the these 3 curves, $\int_{565}^{605} L_w(\lambda)\, d\lambda$, is the same, 1.19×10^{-4} W m^{-2} sr^{-1}, to within a fraction of 1 percent. This shows that the total Raman scattered energy is the same regardless of the wavelength band resolution. Second, the shape of the Raman-emitted L_w is not quite the same as the shape of the emission function seen in Fig. 1. Note that the ratio of the peak value near 584 nm to the "shoulder" value at 580 is less for L_w (about 1.04) than for the emission spectrum (about 1.2). This is because the emission function of Fig. 1 is the shape of the spectrum emitted at any particular depth in the water, whereas the shape of the L_w curve is determined by contributions from the entire water column, *as altered by the wavelength-dependent absorption of the water column.*

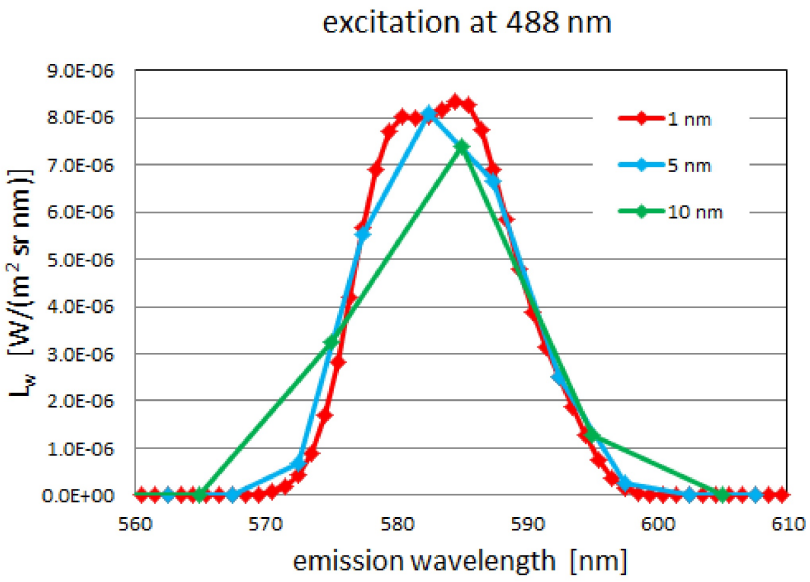

Fig. 2. EcoLight-computed Raman water-leaving radiances induced by a lidar input of 1 W m^{-2} at 488 nm, for three different band widths in the emission region.

Absorption by pure water increases by a factor of three (from 0.08 to 0.24 m^{-1}) between 570 and 600 nm, and by 18% (from 0.090 to 0.106 m^{-1}) between 580 and 584 nm. The rapidly increasing absorption values change the shape of the local (at each depth) emission function when integrated over depth to obtain the total L_w, which has contributions from all depths. Simply stated, the higher absorption at the 584 nm peak lets relatively less of the radiance make it to the surface than for the shoulder at 580 nm, so the peak appears smaller relative to the shoulder than what is seen for the emission function of Fig. 1.

The effect of absorption on the shape of the Raman-emitted radiance can be seen more dramatically in Fig. 3. This figure shows the downwelling (i.e., seen looking upward) Raman radiance, L_d, for selected depths in the water. Just below the level sea surface at depth $z = 0$, the downwelling radiance is just the upwelling radiance reflected downward by the sea surface. By a depth of 5 m, there is now enough water above to generate a downwelling radiance that looks very similar to the emission function. This L_d continues to build up as the water layer above becomes thicker, until the maximum L_d is reached at about 20 m depth. Below that, L_d decreases with depth at the excitation irradiance reaching depth at 488 nm continues to decrease, and absorption removes more of the L_d generated near the sea surface. Note that the larger absorption at 584 nm removes so much of the radiance generated near the surface that by 40 m the radiance at 584 actually becomes less than at the original shoulder at 580. The shape of the L_d emission then begins to look somewhat like an excitation function, with the peak on the left and the shoulder on the right. This transformation of the shape of the emitted radiance is due entirely to the wavelength dependence of the absorption.

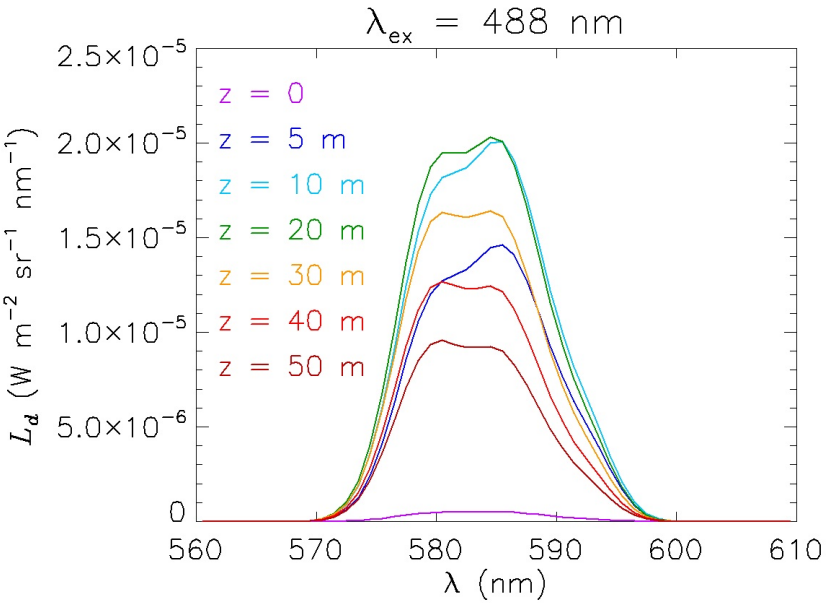

Fig. 3. Downwelling Raman-scattered radiance as a function of depth. The shape of L_d depends on depth because of wavelength-dependent absorption.

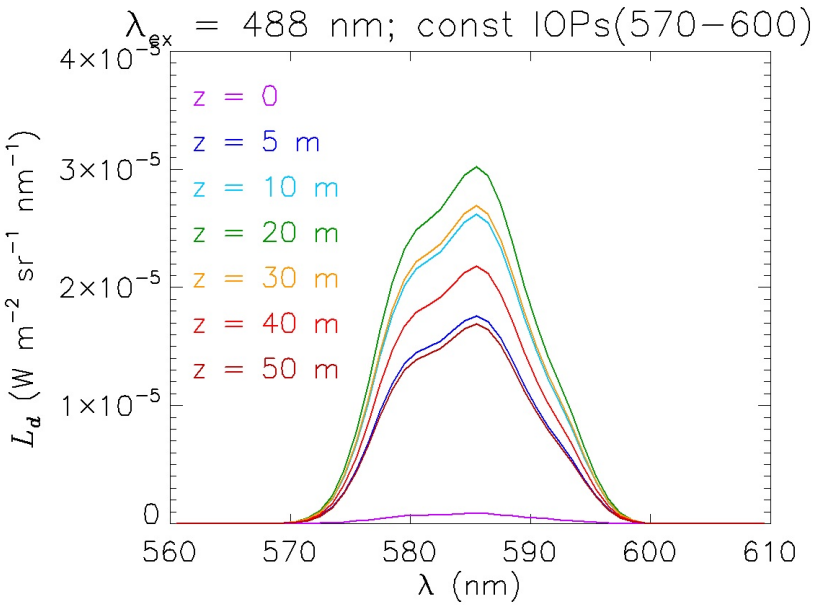

Fig. 4. Downwelling Raman-scattered radiance as a function of depth for the case of artificial water IOPs having the same values from 570 to 600 nm. The shape of L_d is now independent of depth and is the same as the Raman-emission function of Fig. 1.

This claim can be verified as follows. I created an "artificial water" IOP data file with the IOP values between 570 and 600 nm having the values at 570 nm. The water IOPs are then the same over the range of emission wavelengths seen in Fig. 3. The resulting Raman L_d spectra are seen in Fig. 4. Now, without the wavelength-dependent absorption, the shape of L_d does not change with depth and, indeed, looks exactly like the shape of the emission function seen in Fig. 1. The magnitude of the L_d curves is greater than before because the absorption is less. The shape of the L_u emission (not shown) looks similar to that of L_w and does not change much with depth. The reason is that at a given depth L_u comes mostly from depths not much deeper, because there is little light at great depths, so absorption over large distances has less chance to alter the shape of the curve.

These simulations show that the interpretation of Raman-scattered spectra is complicated because of IOP effects at both the excitation and emission wavelengths, even in the simplest possible case of excitation at one wavelength in an otherwise black sky. The situation becomes even more complicated for solar-stimulated inelastic scatter because many excitation wavelengths can contribute to a range of emission wavelengths, and everything blurs together in a non-obvious fashion.

A Simple Model for Band-averaged Raman Scatter

This section develops an approximate analytical model for band-integrated Raman contributions to water-leaving radiance or remote-sensing reflectance. This model will be used to understand and check H numerical simulations.

Consider, as above, an excitation irradiance onto the sea surface of $E_d(488)$ in W m^{-2} nm^{-1} over a 1 nm wide band, which gives a total input irradiance of $E_d(z{=}0,488)$ in W m^{-2} at the sea surface. This irradiance propagates to depth according to

$$E_d(z,488) = E_d(0,488)\exp[-K_d(488)\,z]\,, \tag{2}$$

if $K_d(z,488)$ is assumed to be independent of depth z (which, of course, is never quite correct). At each depth z, the amount of $E_d(z,488)$ that Raman scatters into *all* wavelengths is determined by the Raman scattering coefficient $b^R(488)$ according to

$$S^R(z,\Delta\lambda) = E_d(z,488)\,b^R(488)\,, \tag{3}$$

where $\Delta\lambda$ denotes the bandwidth receiving the scattered power, and S^R (with units of W m^{-3}) is a source term over the emission wavelengths. Figure 1 shows that the emission is centered near 583 nm and $\Delta\lambda \approx 15$ nm. Equation (1) shows that Raman scattering is roughly isotropic (to within 55%), in which case the scattered-power source term of Eq. (3) can be approximated as an isotropic source term for band-averaged scattered spectral radiance over the emission band, which is approximately applicable at the 583 nm center of the emission band:

$$S_L^R(z,583) = \frac{S^R(z,\Delta\lambda)}{4\pi\,\Delta\lambda}. \tag{4}$$

This source function can be used to compute the upwelling spectral radiance at 583 nm just below the sea surface, generated by Raman scattering at all depths:

$$L_u^R(0,583) = \int_0^\infty S_L^R(z,583)\, e^{-K_{Lu}(583)\,z}\, dz \tag{5}$$

$$= \frac{E_d(0,488)\, b^R(488)}{4\pi\,\Delta\lambda} \int_0^\infty e^{-K_d(488)z}\, e^{-K_{Lu}(583)z}\, dz$$

$$= \frac{E_d(0,488)\, b^R(488)}{4\pi\,\Delta\lambda\,[K_d(488) + K_{Lu}(583)]}. \tag{6}$$

In Eq. (4), $K_{Lu}(z,583)$ has been assumed independent of depth, and Eqs. (2)-(4) have been used in going from Eq. (5) to (6). The water-leaving radiance $L_w{}^R = L_u{}^R(z{=}0)/n^2$, where $n = 1.34$ is the index of refraction of water. Thus the final model for Raman water-leaving radiance at 583 nm induced by excitation at a single wavelength of 488 nm is

$$L_w^R(583) = \frac{E_d(0,488)\, b^R(488)}{4\pi\, n^2\,\Delta\lambda\,[K_d(488) + K_{Lu}(583)]}. \tag{7}$$

Equation (7) will be used below to check the numerical computation of lidar-induced Raman scatter.

However, for solar-stimulated Raman scatter the total upwelling radiance at 583 contains contributions from all wavelengths in a bandwidth $\Delta\lambda'$ centered near 488. Thus the total $L_w{}^R(583)$ is Eq. (7) times $\Delta\lambda'$, assuming that b^R, E_d and K_d for the narrow band $\Delta\lambda' \approx 10$ nm are roughly equal to their values at 488.

Finally, the solar-stimulated Raman contribution to the band-averaged remote-sensing reflectance near 583 is $R_{rs}{}^R(583) = L_w{}^R(583)/E_d(\text{air}, 583)$, or

$$R_{rs}^R(583) = \frac{1}{4\pi n^2}\, \frac{b^R(488)}{[K_d(488) + K_{Lu}(583)]}\, \frac{\Delta\lambda'}{\Delta\lambda}\, \frac{E_d(0,488)}{E_d(air,583)}. \tag{8}$$

In this equation, all quantities at 488 are approximated as averages over the excitation band $\Delta\lambda'$ centered at 488, and all quantities at 583 are band averages over the emission band $\Delta\lambda$ centered at 583 nm. This equation will be used below to check numerical predictions of solar-stimulated $R_{rs}{}^R$.

The EcoLight runs that generated Fig. 2 also show that $K_d(z,488)$ varied from about 0.024 m^{-1} near the surface to 0.026 m^{-1} at 50 m depth. Likewise, $K_{Lu}(z,583)$ varied from about 0.0269 m^{-1} near the surface to 0.0267 m^{-1} at 50 m. Approximating these K functions by 0.025 and 0.027 m^{-1}, respectively, and using the above values for the other factors in Eq. (7) gives a final estimate of

$$L_w^R(583) \approx \frac{E_d(0,488)\, b^R(488)}{4\pi n^2 \Delta\lambda\, [K_d(488) + K_{Lu}(583)]}$$

$$= \frac{(1)\,(2.4\times10^{-4})}{4\pi\,(1.34)^2\,(15)\,(0.025+0.027)}$$

$$= 13.6\times10^{-6}\ \mathrm{W\,m^{-2}\,sr^{-1}\,nm^{-1}}.$$

This value is about 70% greater than the EcoLight values of about 8×10^{-6} near the center of the emission band. Considering the crudeness of the approximations used to derive Eq. (7), a factor-of-two agreement with the numerically computed Raman-generated $L_w^R(583)$ seen in Fig. 2 is reasonable.

Simulation of the Solar-Stimulated Raman Contribution to Remote-Sensing Reflectance

EcoLight was next used to simulate solar-induced remote-sensing reflectance R_{rs} without any inelastic scattering, using the following inputs for very clear Case 1 ocean water:

Chl = 0.02 mg m^{-3} in the "new Case 1" IOP model
sun at 30 deg zenith angle in a clear sky
infinitely deep water with the RTE solved down to 50 m
10 nm wavelength bands from 470 to 610 nm

The 10 nm bandwidth is typical of what is used in most HydroLight runs. Selected results for this run, as will be needed below, are

E_d(0,480-490) = 1.4369 W m^{-2} nm^{-1} (the band-averaged spectral irradiance over 480-490 nm)
E_d(air,580-590) = 1.3654 W m^{-2} nm^{-1} (the band-averaged spectral irradiance over 580-590 nm)
K_d(480-490) = 0.0222 m^{-1} (average over the upper 10 m of the water column)
K_{Lu}(580-590) = 0.1231 m^{-1} (average over the upper 10 m of the water column)
R_{rs}(580-590) = 4.682 x10^{-4} sr^{-1} (the band-averaged R_{rs} over 580-590 nm)

I then repeated this run with all inputs being the same, except that I included Raman scatter. The quantities that differed are

K_{Lu}(580-590) = 0.0986 m^{-1} (average over the upper 10 m of the water column)
R_{rs}(580-590) = 5.571 x10^{-4} sr^{-1} (the band averaged R_{rs} over 580-590 nm)

The increase in R_{rs}(580-590) as computed with Raman is R_{rs}^R = 8.89 x10^{-5} sr^{-1}, which is about 19% more than the value without Raman scattering. This is consistent with other estimates (Morel et al., 2002) of the contribution of Raman scatter to remote-sensing reflectance in very clear waters.

This numerically computed Raman contribution to $R_{rs}(580\text{-}590)$ can be compared with the simple model of Eq. (8), using the values just given:

$$R_{rs}^{R}(583) \approx \frac{1}{4\pi n^2} \frac{b^{R}(488)}{[K_d(488) + K_{Lu}(583)]} \frac{\Delta\lambda'}{\Delta\lambda} \frac{E_d(0,488)}{E_d(air,583)}$$

$$= \frac{1}{4\pi\,(1.34)^2} \frac{2.4\times10^{-4}}{(0.022+0.099)} \frac{10}{15} \frac{1.437}{1.365} \quad .$$

$$= 5.9\times10^{-5}\ \mathrm{sr}^{-1} .$$

Here I have used 10 and 15 nm for the excitation and emission bandwidths, respectively, as shown in Fig. 1. This is once again reasonably good agreement between the simple model and the numerical calculations, given the crudeness of the estimates used in developing the model of Eq. (8) and the approximate numerical values used therein.

Lee et al. (1994) derived a somewhat more sophisticated (but still assuming isotropic Raman scattering) approximate model for the contribution of Raman scatter to R_{rs} (their Eq. B12):

$$R_{rs}^{R}(\lambda) = 0.072 \frac{b^{R}(\lambda') E_d(air,\lambda')}{[2a(\lambda) + a(\lambda')] E_d(air,\lambda)} ,$$

where a is the total absorption coefficient. Using the values of $a(488) = 0.021$ m^{-1} and $a(583) = 0.11$ m^{-1} for the present simulation gives $R_{rs}^{R} = 7.5 \times 10^{-5}$ sr^{-1}, which is in even better agreement with the numerical value.

These calculations indicate that HydroLight is both evaluating the Raman equations correctly for given wavelengths, and properly integrating the equations over the user-selected wavelength bands used in a HydroLight or EcoLight run. HydroLight and EcoLight of course include the effects of wavelength-dependent IOPs and multiple scattering.

HydroLight-EcoLight v 5.1.4

This version of the code was finalized in December 2011. The code now allows users to select the wavelength dependence of the Raman scattering coefficient in the User Interface, and it has a few other internal changes to improve the Raman calculations. I recommend using this version if you are doing calculations where Raman scatter is significant (e.g., in very clear waters). There were enough changes to the previous version to make it easier to send out a new CD than to upload a patch on the Users' Group website. Let me know if you want the upgrade.

Acknowledgements

Emmanuel Boss and Dong Sun both asked penetrating questions about HydroLight's Raman calculations, which led me to prepare these notes. Many thanks to them!

References

Bartlett, J. S., K. J. Voss, S. Sathyendranath, and A. Vodacek, 1998. Raman scattering by pure water and seawater. *Appl. Optics* 37(15), 3324-3332.

Desiderio, R. A., 2000. Application of the Raman scattering coefficient of water to calculations in marine optics. *Appl. Optics* 39(12), 1893-1894.

Ge, Y., H. R. Gordon, and K. J. Voss, 1993. Simulation of inelastic-scattering contributions to the irradiance field in the ocean: variation in Fraunhofer line depths. *Appl. Optics* 32, 4028-4036.

Kattawar, G. W. and X. Xu, 1992. Filling in of Fraunhofer lines in the ocean by Raman scattering. *Appl. Optics* 31(30), 6491-6500.

Lee, Z.-P., K. L. Carder, S. K. Hawes, R. G. Steward, T. G. Peacock, and C. O. Davis, 1994. Model for the interpretation of hyperspectral remote-sensing reflectance. *Appl. Optics* 33(24), 5721-5732.

Morel, A., D. Antoine, and B. Gentili, 2002. Bidirectional reflectance of oceanic water: accounting for Raman emission and varying particle scattering phase function. *Appl. Optics* 41(30), 6289-6406.

Walrafen, G. E., 1967. Raman spectral studies of the effects of temperature on water structure. *J. Chem. Phys.* 47(1), 118-121.

Appendix A. Raman Equations with *Light and Water* Typos Corrected

The Raman wavelength distribution function $f^R(\lambda' \rightarrow \lambda)$ is most conveniently described in terms of the corresponding *wavenumber* distribution function $f^R(\kappa'')$, where κ'' is the *wavenumber shift*, expressed in units of cm^{-1}. This follows because the Raman-scattered light undergoes a *frequency* shift that is independent of the incident frequency. The wavenumber κ in cm^{-1} is related to the wavelength λ in nm by $\kappa = 10^7/\lambda$, and to the frequency ν by $\kappa = \nu/c$, where c is the speed of light.

According to Walrafen (1967), the shape of $f^R(\kappa'')$ for water is given by a sum of four Gaussian functions:

$$f^R(\kappa'') = \left[\left(\frac{\pi}{4\ln 2}\right)^{\frac{1}{2}} \sum_{i=1}^{4} A_i\right]^{-1} \sum_{j=1}^{4} A_j \frac{1}{\Delta\kappa_j} \exp\left[-4\ln 2 \frac{(\kappa'' - \kappa_j)^2}{\Delta\kappa_j^2}\right] \quad (\text{cm}), \qquad \text{(L\&W 5.92)}$$

where

$\kappa'' =$ the wavenumber shift of the Raman-scattered light, *relative to the wavenumber* κ' *of the incident light*

$\kappa_j =$ the center of the j^{th} Gaussian function, in cm^{-1}

$\Delta\kappa_j =$ the full width at half maximum of the j^{th} Gaussian function, in cm^{-1}

$A_j =$ the nondimensional weight of the j^{th} Gaussian function.

The values of A_j, κ_j, and $\Delta\kappa_j$ for pure water at a temperature of 25° C are given in L&W Tab. 5.3:

Table 5.3. Parameter values for the Raman wavenumber distribution function $f^R(\kappa'')$ of Eq. (5.92), for pure water at a temperature of 25° C. Data from Walrafen (1969). (Kattawar and Xu (1992) use somewhat different values, but the differences are indistinguishable in plots of f^R.)

j	A_j	κ_j (cm^{-1})	$\Delta\kappa_j$ (cm^{-1})
1	0.41	3250	210
2	0.39	3425	175
3	0.10	3530	140
4	0.10	3625	140

The function $f^R(\kappa'')$ can be interpreted as a probability density function giving the probability that a photon of any incident wavenumber $\kappa' = 10^7/\lambda'$, if Raman scattered, will be scattered to a wavenumber

$$\kappa = \kappa' - \kappa''.$$

A change of variables from κ'' to λ' in Eq. (5.92) (see page 296 of the CD version of *Light and Water*, which has the typos of the hardcopy corrected) gives the corresponding *wavelength* distribution function $f^R(\lambda' \to \lambda)$

$$f^R(\lambda' \to \lambda) \equiv \begin{cases} \dfrac{10^7}{\lambda^2} f^R\left(\dfrac{10^7}{\lambda''}\right) = \dfrac{10^7}{\lambda^2} f^R\left[10^7\left(\dfrac{1}{\lambda'} - \dfrac{1}{\lambda}\right)\right] & \text{if } \lambda' < \lambda, \\ 0 \quad \text{if } \lambda' \geq \lambda, \end{cases} \qquad \text{(L\&W 5.94, corrected)}$$

where the wavelengths are now in nm. This is the function plotted in Fig. 1. Note that

$$\int_0^{\kappa'} f^R(\kappa'')\, d\kappa'' \equiv \int_{\lambda'}^{\infty} f^R(\lambda' \to \lambda)\, d\lambda = 1,$$

as required of a probability distribution function.